PHOTONIC SENSORS / Vol. 10, No. 2, 2020: 155–161

Study of Utilization of Embedded Metal Nanoparticles in Dielectric Thin Film for Humidity Sensing

Hala J. EL-KHOZONDAR[1] and Waleed S. MOHAMMED[2]

[1]*Islamic University of Gaza, Electrical Engineering Department, Gaza-108, Palestine*

[2]*Bangkok University, BU-CROCCS, School Of Engineering, Pathumthani 12120, Thailand*

[*]Corresponding author: Waleed S. MOHAMMED E-mail: wsoliman@gmail.com

Abstract: This paper presents a theoretical study of the utilization of the shift in the reflection peak of the thin dielectric film with embedded metal nanoparticles (NPs) towards humidity and vapor applications. The presence of the NPs in the film results in a complex effective index. Hence, the reflected light at the superstrate-film interface causes a phase shift when the index of the surrounding is changed. This alters the reflected spectrum of the formed Fabry-Perot, for both the reflection peak wavelength and intensity. Here, the dynamic range of the proposed sensor is optimized through the variation of the film thickness and nanoparticle metal type, as well as the volume fraction.

Keywords: Nanoparticles; polymer film; humidity sensor

Citation: Hala J. EL-KHOZONDAR and Waleed S. MOHAMMED, "Study of Utilization of Embedded Metal Nanoparticles in Dielectric Thin Film for Humidity Sensing," *Photonic Sensors*, 2020, 10(2): 155–161.

1. Introduction

Monitoring humidity is essential for comprehensive applications in electronic and chemical industries, optoelectronics devices, agriculture, medical diagnoses, metrology, and aerospace [1, 2]. To adapt a comfortable life to human beings, it is important to control humidity levels inside buildings, cars, shops, and other places [3]. Therefore, it is necessary to monitor and measure humidity using low-cost, small-size, high-stability, and high-sensitivity humidity sensors. The development of humidity sensors differs according to the type of the structural material, e.g., organic and inorganic materials. Inorganic materials used in the fabrication of humidity sensor take different forms including nanowires [4], nanotubes [5], and nanofiber [6]. Organic and composite materials, such as nafion persulphonate, are used to fabricate the humidity sensors [7]. In addition, there are graphene oxide [8] and plasmonic materials [9] based sensors. These sensors work at different mechanisms including changes of the resistivity, capacity, optical properties, piezoresistivity, magnetism, and frequency (impedance) of the active material with the humidity level [6, 10].

Nanomaterials' distinctive optical, mechanical, electrical, and magnetic properties make them a vital candidate for many applications including but not limited to sensors [1], solar cells [11, 12], optoelectronic devices [13], and waveguides [14]. In particular, the sensor technology has a high leap in the technology world due to the use of nanotechnology and nanomaterials. This leads to an encroachment in the field of humidity sensors [15].

Received: 5 May 2019 / Revised: 9 August 2019

DOI: 10.1007/s13320-019-0570-9
Article type: Regular

Several types of nanoparticles (NPs) are used in fabricating the humidity sensor. For example, flexible impedance-type humidity sensors by using gold (Au) NPs in different nanocomposites are presented by different authors, e.g., in [16]. Silver (Ag) NPs in various nanocomposites are used to synthesize humidity sensors [17–19]. These sensors have been developed in different ways such as the chemical reduction process [17], the electrostatic spray deposition technique [18], and the vacuum deposition process [19]. Different parameters have been studied in the development of these sensors. Some considered the ageing of nanocomposite coatings and the influence of an aqueous environment on their internal structure properties [19]. The others considered the influence of the deposition times on properties of films [18].

Adhyapak *et al*. [20] used Au(c)-Ag(s) bimetallic NPs to fabricate resistors on ceramic rods to measure relative humidity response. Titanium dioxide (TiO_2) NPs that have a high surface area are waved in different nanostructures to build high sensitivity humidity sensor, i.e., LiCl-doped TiO_2 NPs sensors [2]. Other structures like CuO NPs [3], ZnO nanorods [21], and nickel (Ni) NPs [22] are also used to structure humidity sensors. In this work, we theoretically propose a device for humidity/vapor detection in air by the optimization of the shift in the reflection peak from a thin polymer film with different types of NPs impurities. Section 2 introduces the proposed humidity sensor. Section 3 presents the calculation results followed by conclusions in Section 4.

2. Proposed humidity sensing scheme

In this theoretical study, a simple alternative approach is used by utilizing the shift in the reflection peak from metal NPs impeded in a polymer host thin film that is coated on a glass substrate as illustrated in Fig. 1. The presence of metal NPs results in a complex effective index, n_{eff}, of the thin film.

$$n_{\text{eff}}^2 = \varepsilon_h \frac{1-2fa}{1+2fa} \tag{1}$$

where $a=(\varepsilon_m-\varepsilon_h)/(\varepsilon_m+2\varepsilon_h)$. In (1), ε_h is the host polymer permittivity, ε_m is the NP metal permittivity, and f is the NP filling factor [23]. In the analysis, the effective index is calculated by using Maxwell's Garnett effective medium theory where the particles' sizes are assumed to be much smaller than the optical wavelength [24].

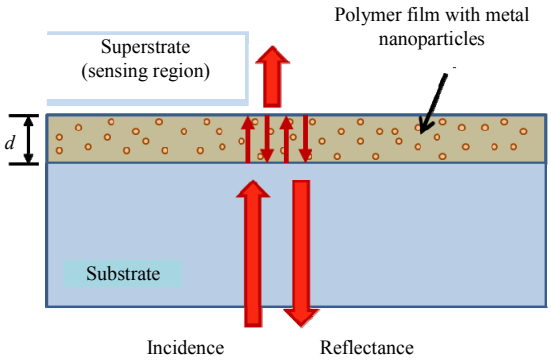

Fig. 1 Proposed humidity sensor: nanocomposite with thickness d is coated on a glass substrate.

When light is normally incidental, multiple reflections inside the film with NPs form a Fabry-Perot where the reflection coefficients at the film/substrate (r_{21}) and film/superstrate (r_{23}) are complex. The resulted reflection coefficient, r, is

$$r = r_{12} + \frac{t_{12}t_{21}r_{23}\exp\left(\mathrm{i}2\mathrm{k}_0 n_{\text{eff}} d\right)}{1-r_{23}r_{21}\exp\left(\mathrm{i}2\mathrm{k}_0 n_{\text{eff}} d\right)} \tag{2}$$

where

$$r_{21} = -r_{12} = (\psi_2 n_{\text{eff}} - \psi_1 n_1)/(\psi_2 n_{\text{eff}} + \psi_1 n_1)$$

$$r_{23} = (\psi_2 n_{\text{eff}} - \psi_3 n_3)/(\psi_2 n_{\text{eff}} + \psi_3 n_3)$$

$$t_{mj} = 1 + r_{mj}$$

where m and j can be 1, 2 or 3. The refractive indices n_1 and n_3 are for the substrate and superstrate, respectively. The coefficient ψ_j=1 is for TE polarization and ψ_j=1/ε_j is for TM polarization. In (2), the term added to r_{12} on the right hand side depends on the Fresnel reflection and transmission at the two interfaces (film-substrate and film-superstrate) as well as the propagation/attenuation inside the film. The constant

k_0 is the free space propagation constant. These coefficients are complex in nature due to the absorption of the metal NPs.

The proposed model in Fig. 1 assumes a glass substrate with fixed index n_1. The superstrate index, n_3, however changes with the presence of vapor; n_3 becomes an effective index composed of air with certain concentration of water. Its value ranges from 1 to a maximum of 1.33. The change of n_3 due to humidity alters the complex Fresnel reflection coefficient at the superstrate-film interface (r_{23}). This causes a shift in the amplitude and phase of the term added to r_{12} on the right side of (2). Hence, it changes the total reflection coefficient, r. This by its turn affects the reflection spectrum in terms of the peak wavelength location and the maximum amplitude as illustrated in Fig. 2. The plots are calculated for gold NPs in a polymer (n_h = 1.446) and a glass substrate (n_1 = 1.5) for f = 0.06 when TE wave is considered.

The calculated reflectance shows a reduction in the amplitude when n_3 increases from air (n_3 = 1) towards water (n_3 = 1.33). There is also a clear blue-shift in the peak wavelength. In order to optimize the response of the structure, two figures of merit are introduced as defined in (3a) and (3b).

$$Intensity\ dynamic\ range = R_{\max,\mathrm{air}} - R_{\max,\mathrm{water}} \quad (3a)$$

$$Wavelength\ dynamic\ range = \lambda_{\max,\mathrm{air}} - \lambda_{\max,\mathrm{water}}. \quad (3b)$$

Three parameters are varied in this study: the type of metal NPs, the film thickness d, and the NP filling factor f.

It is worth mentioning that in the presented analysis, the change of the effective index around the NPs due to polymer swelling [25] or porosity in the host medium [26] is not considered. Only changes on the film surface are considered to cause a shift in the complex Fresnel reflection and hence the total Fabry-Perot reflectance spectrum. This is shown by the blue-shift in the reflection peak when an increase in the superstrate index is depicted in Fig. 2. This trend is opposite to the typical red-shift observed when the host medium index is increased by the change of the surrounding, duty porosity in the nanocomposite film.

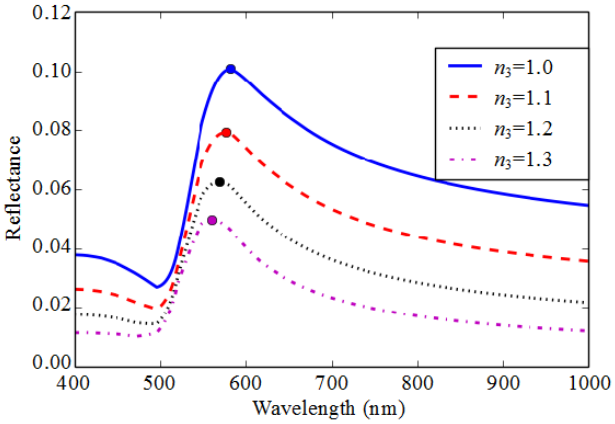

Fig. 2 Reflectance as the function of wavelength at different values of refractive index (n_3) while the film thickness is kept fixed (d = 80 nm). In this case, Au NP is used in the nanocomposite with filling factor f = 0.06.

3. Calculation results

The optimization process aims at maximizing the dynamic ranges through comparing different metal NPs inclusions as well as film thickness d and volume fraction f. Gold NPs are first tested when varying d and f as shown in Fig. 3. The plots in Fig. 3(a) indicate that the value of film thickness d, which causes the maximum peak reflection $R_{\max}$, decreases as the value of the filling factor f increases. This is logical as higher f causes larger absorption in the effective film. For example, for f between 0.05 and 0.06, d of 80 nm causes the highest $R_{\max}$. For f = 0.09, d causes that the highest $R_{\max}$ decreases to 70 nm. Here, $R_{\max}$ is calculated at n_3=1. Figures 3(b) and 3(c) show that the wavelength dynamic range is maximized for d less than 40 nm. However, the intensity dynamic range is higher for d > 90 nm.

The changes of the wavelength and peak reflectance for these two limits are depicted in Fig. 4 for a volume fraction, f = 0.055. Here, $R_{\max}$ is maximized for the higher film thickness when compared with gold (100 nm for f between 0.05 and 0.06). The intensity dynamic range is shown to increase for the higher thickness reaching a peak

similar to that of R_{max}. The plots in Figs. 4(c) and 4(d) show the calculated sensitivities for the peak amplitude detection and peak wavelength detection for the two selected film thicknesses.

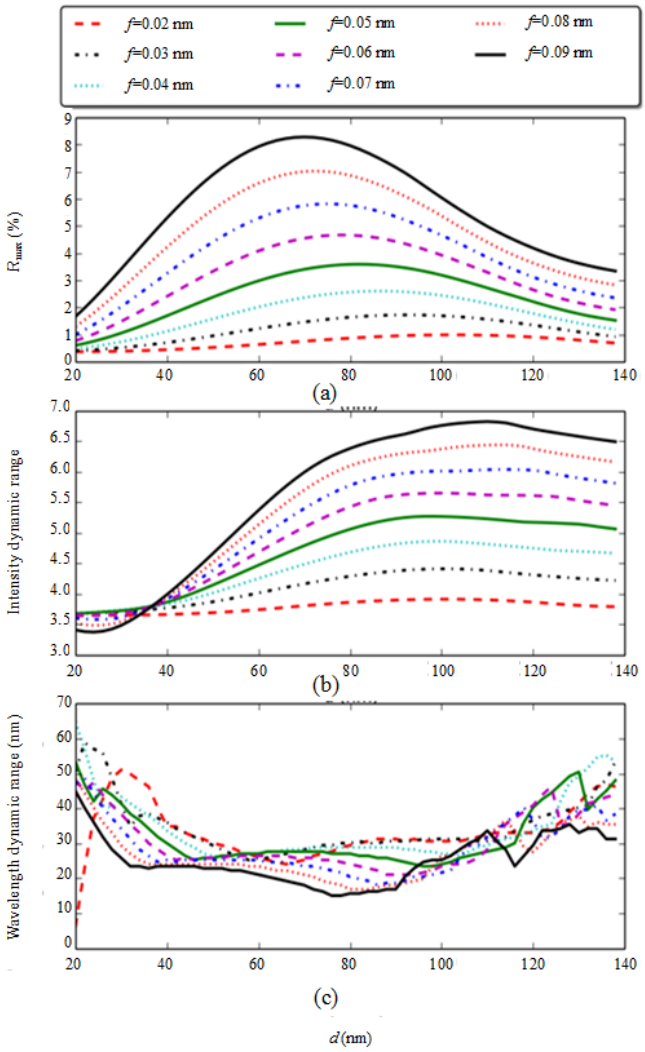

Fig. 3 Calculated (a) reflection peak, (b) intensity dynamic range, and (c) wavelength dynamic range as the function of the film thickness, d, at different volume fractions, f, for Au NPs in polymer (n_h = 1.466).

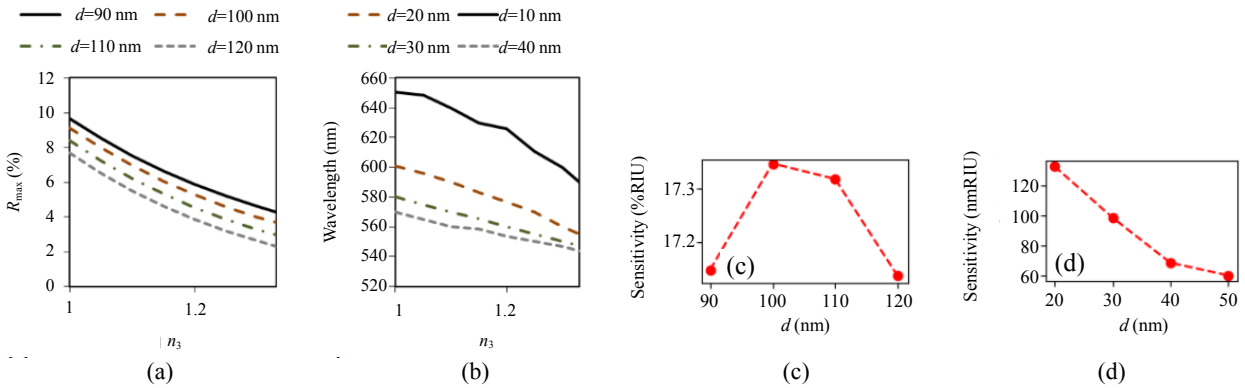

Fig. 4 Change of the (a) peak intensity for d > 90 nm and (b) peak wavelength for d < 40 nm for Au NPs in polymer when volume fraction f is set to be 0.055; (c) sensitivity for the peak intensity detection and (d) sensitivity for peak wavelength detection.

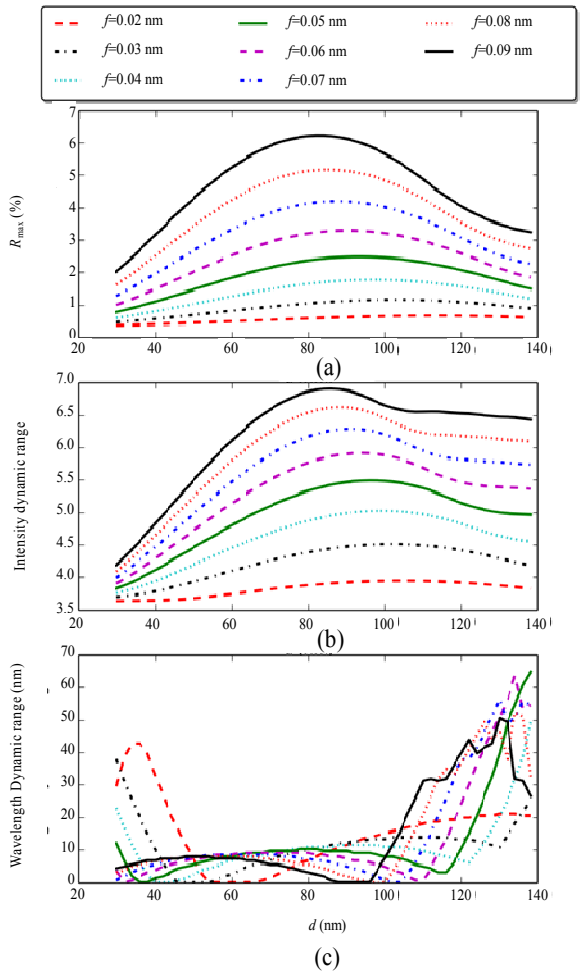

Fig. 5 Calculated (a) reflection peak, (b) intensity dynamic range, and (c) wavelength dynamic range as the function of the film thickness, d, at different volume fractions, f, for Au NPs in polymer(n_h = 1.466).

The sensitivity duty peak amplitude seems to be almost constant for different thicknesses. However, the sensitivity due to the change of the peak wavelength with superstrate index decreases for larger thickness. The wavelength dynamic range in Fig. 5(c), however, shows three distinctive regions: high dynamics and low d, low dynamics, and a second high dynamics at high d. As illustrated in Fig. 6, high wavelength dynamic is caused by the broadening of the plasmonic peak for both the low and high film thicknesses. This is not the case when the peak is defined as in Fig. 6(b).

For the sake of comparison, the calculations have been repeated for Ni NPs. Figure 7 displays the intensity dynamic range as the function of d at different values of f. It can be seen that for $d > 50$ nm and $f > 0.03$ the intensity increases as f and d increase. At a low volume fraction such as $f = 0.02$, the intensity dynamic range decreases as d increases to reach the minimum at $d = 110$ nm. The inset of Fig. 7 shows the reflection at different values of n_3 as the function of the wavelength. It can be seen clearly that as n_3 goes from pure air to pure water, a decrease follows in the peak accompanied with blue shift for $d = 80$ nm.

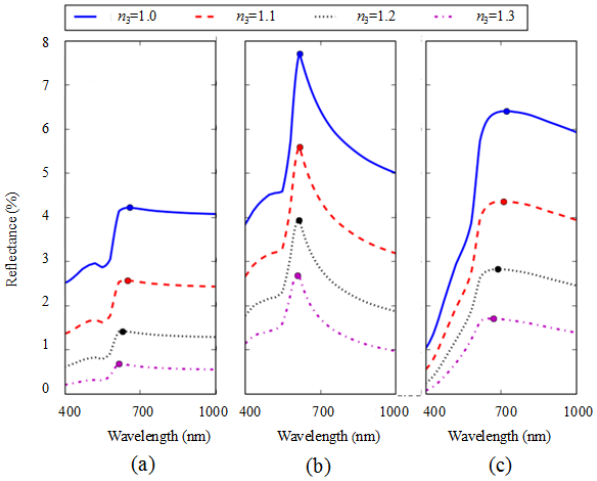

Fig. 6 Calculated reflection spectrum for Cu NPs in polymer with f=0.05 at the film thicknesses of (a) 20 nm, (b) 80 nm, and (c) 140 nm.

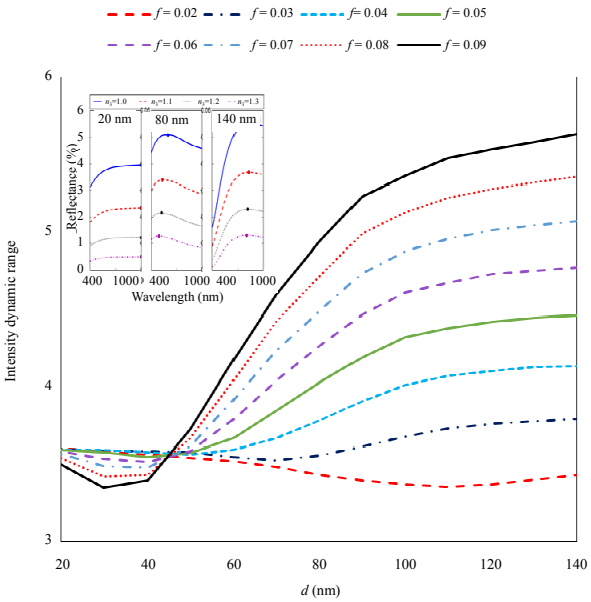

Fig. 7 Intensity dynamic range as the function of film thickness d at different values of filling factor, f, for Ni NPs in polymer (n_h =1.466). The inset shows the calculated reflection spectrum for Ni NPs in polymer with f = 0.05 at the film thicknesses of 20 nm, 80 nm, and 140 nm for different values of n_3.

Comparing the intensity dynamic values for the three nanoparticles, the dynamic range dependency on the film thickness and volume fraction seems to follow a similar trend for Au and Cu. This is however different in the case of Ni where a more dramatic change is observed when moving from lower to higher thicknesses. This can be due to high absorption of Ni nanoparticles.

4. Conclusions

In this work, a humidity sensor is proposed by using NPs hosted in polymer as a film layer on the top of glass substrate and covered by air superstrate. The NPs, which are used in this calculation, are Au, Cu, and Ni. The effect of changing the type of NPs, the filling factor, and the thickness of the film on the performance of the sensor is studied extensively. The calculation results for the three metals indicate that a film thickness between 70 nm and 100 nm results in the maximum intensity dynamic range for volume fractions more than 0.05. Sharp plasmonic peaks are also presented within the same operation region for Au and Cu giving wavelength dynamic ranges around 20 nm and 10 nm, respectively. Higher wavelength dynamic ranges can be achieved for the thinner film. However, the plasmonic peak for the thin film has a broader spectrum and hence can cause a large error in detection. Hence, for practicalities, a thickness range between 70 nm and 100 nm should be suitable for operation in both the intensity and wavelength modulations for the given host medium and metals.

Acknowledgement

The authors would like to acknowledge the colleagues in the Electrical Engineering Department, Islamic University of Gaza, Gaza, Palestine, for their support and help.

References

[1] A. M. Gurban, D. Burtan, L. Rotariu, and C. Bala, "Manganese oxide based screen-printed sensor for xenoestrogens detection," *Sensors & Actuators B: Chemical*, 2015, 210: 273–280.

[2] A. I. Buvailo, Y. Xing, J. Hines, N. Dollahon, and E. Borguet, "TiO_2/LiCl-based nanostructured thin film for humidity sensor applications," *ACS Applied Materials & Interfaces*, 2011, 3(2): 528–533.

[3] I. S. Yakubu, U. Muhammad, and A. A. Muhammad, "Humidity sensing study of polyaniline/copper oxide nanocomposites," *International Journal of Advanced Academic Research Sciences*: *Technology & Engineering*, 2018, 4(5): 49–61.

[4] Q. Kuang, C. Lao, Z. L. Wang, Z. Xie, and L. Zheng, "High-sensitivity humidity sensor based on a single SnO_2 nanowire," *Journal of the American Chemical Society*, 2007, 129(19): 6070–6071.

[5] B. Cheng, B. Tian, C. Xie, Y. Xiao, and S. Lei, "Highly sensitive humidity sensor based on amorphous Al_2O_3 nanotubes," *Journal of Materials Chemistry*, 2011, 21(6): 1907–1912.

[6] U. Mogera, A. A. Sagade, S. J. George, and G. U. Kulkarni, "Ultrafast response humidity sensor using supramolecular nanofibre and its application in monitoring breath humidity and flow," *Scientific Reports*, 2014, 4: 1–9.

[7] P. Kuban, J. M. Berg, and P. K. Dasgupta, "Durable microfabricated high-speed humidity sensors," *Analytical Chemistry*, 2004, 76(9): 2561–2567.

[8] S. Borini, R. White, D. Wei, M. Astley, S. Haque, E. Spigone, *et al.*, "Ultrafast graphene oxide humidity sensors," *ACS Nano*, 2013, 7(12): 11166–11173.

[9] J. J. Steele, N. T. Taschuk, and M. J. Brett, "Nanostructured metal oxide thin films for humidity sensors," *IEEE Sensors Journal*, 2008, 8(8): 1422–1429.

[10] H. Farahani, R. Wagiran, and M. N. Hamidon, "Humidity sensors principle, mechanism, and fabrication technologies: a comprehensive review," *Sensors*, 2014, 14(5): 7881–7939.

[11] H. J. El-Khozondar, R. J. El-Khozondar, M. M. Shabat, and D. Schaadt, "Solar cell with multilayer structure based on nanoparticles composite," *Optik*, 2018, 166: 127–131.

[12] M. K. Hedayati, M. Javaherirahim, A. U. Zillohu, H. J. El-Khozondar, M. Bawa'aneh, A. Lavrinenko, *et al.*, "Photo-driven super perfect absorber as an active metamaterial with a tunable molecular-

plasmonic coupling," *Advanced Optical Materials*, 2014, 2(8): 705–710.

[13] A. B. Djurišić, A. M. C. Ng, and X. Y. Chen, "ZnO nanostructures for optoelectronics: material properties and device applications," *Progress in Quantum Electronics*, 2010, 34(4): 191–259.

[14] T. Cheng, C. Rangan, and J. E. Sipe, "Metallic nanoparticles on waveguide structures: effects on waveguide mode properties and the promise of sensing applications," *Journal of the Optical Society of America B*, 2013, 30(3): 743–765.

[15] Y. Oh, K. Kim, S. Hwang, H. Ahn, J. Oh, and J. Choi, "Recent advances of nanostructure implemented spectroscopic sensors – a brief overview," *Applied Spectroscopy Reviews*, 2016, 51(7–9): 656–668.

[16] H. Lee, C. Wang, and C. Lin, "High-performance humidity sensors utilizing dopamine biomolecule-coated gold nanoparticles," *Sensors and Actuators B*, 2014(191): 204–210.

[17] A. C. Power, A. J. Betts, and J. F. Cassidy, "Silver nanoparticle polymer composite based humidity sensor," *Analyst*, 2010, 135(7): 1645–1652.

[18] T. Thiwawong, K. Onlaor, and B. Tunhoo, "A humidity sensor based on silver nanoparticles thin film prepared by electrostatic spray deposition process," *Advances in Materials Science and Engineering*, 2013: 1–7.

[19] M. Drabik, N. Vogel-Schäuble, M. Heuberger, D. Hegemann, and H. Biederman, "Sensors on textile fibres based on Ag/a-C:H:O nanocomposite coatings," *Nanomaterials and Nanotechnology*, 2013, 3: 1–8.

[20] P. Adhyapak, R. Aiyer, S. R. Dugasani, H. U. Kim, C. K. Song, A. Vinu, *et al*., "Thickness-dependent humidity sensing by poly (vinyl alcohol) stabilized Au-Ag and Ag-Au core-shell bimetallic nanomorph resistors," *Royal Society of Open Science*, 2018, 5(6): 171986.

[21] H. H. M. Yusof, S. W. Harun, K. Dimyati, T. Bora, W. S. Mohammed, and J. Dutta, "Optical dynamic range maximization for humidity sensing by controlling growth of zinc oxide nanorods," *Photonics and Nanostructures – Fundamentals and Applications*, 2018, 30: 57–64.

[22] F. Miao, B. Tao, L. Sun, T. Liu, J. You, L. Wang, *et al*., "Capacitive humidity sensing behavior of ordered Ni/Si microchannel plate nanocomposites," *Sensors and Actuators A: Physical*, 2010, 160(1–2). 48–53.

[23] S. Nielsen, *Food Analysis*, vol. 5. New York: Springer Science & Business Media, 2003.

[24] U. Kreibig and M. Vollmer, *Optical properties of metal clusters*, vol. 25. New York: Springer Science & Business Media, 1995.

[25] C. Santos, R. L. Clarke, M. Braden, F. Guitian, and K. W. M. Davy, "Water absorption characteristics of dental composites incorporating hydroxyapatite filler," *Biomaterials*, 2002, 23(8): 1897–1904.

[26] P. Mohan, R. Shinta, J. Fujiwara, H. Takahashi, D. Mott, Y. Matsumura, *et al*., "Boehmite nanorod/gold nanoparticle nanocomposite film for an easy-to-use optical humidity sensor," *Sensors and Actuators B: Chemical*, 2012, 168: 429–435.